Retrospective Shading Correction: Problem, Methods, and Evaluation

Dejan Tomaževic, Boštjan Likar, Franjo Pernuš
University of Ljubljana
Faculty of Electrical Engineering
Tržaška 25, 1000 Ljubljana, Slovenia
{*dejan.tomazevic, bostjan.likar, franjo.pernus*}*@fe.uni-lj.si*

Abstract *In this paper we address the problem of retrospective shading correction, which is a necessary pre-processing step in many tasks of image analysis. Eight algorithms are implemented and compared. The performance of the algorithms was analysed firstly; on three sets of differently structured synthetic shaded and shading-free images, and secondly; on two sets of real microscopical images acquired by two different acquisition set-ups. The results show that the entropy minimisation (EMI) method outperforms the other methods in terms of the reduction of true intensity variations and preservation of intensity characteristics of the shading-free images. The strength of EMI is especially apparent when applied to images containing large-scale objects.*

1. Introduction

Shading or intensity inhomogeneity is a phenomenon, manifesting itself as an intensity gradient across the filed of view not present in the original scene. Because shading is a smoothly varying function of location it normally has only a minor impact on the visual image interpretation or manual analysis. However, it may have an adverse effect on automatic image processing and analysis. In such cases, the correction of shading is a necessary pre-processing step.

In microscopy, shading [7] can be either object-independent or object-dependent. In the first case, shading arises from imperfections in the image acquisition process and may be corrected by calibration methods. In the later case, shading emerges from imperfect object preparation, such as variable slice thickness in transmission microscopy or a non-planar surface in reflectance microscopy. In this cases it can be corrected only retrospectively, i.e., by using the information of the acquired images.

Over the last decades, a number of retrospective shading correction (RSC) methods were proposed in the literature [1,2,3] but little has been done to evaluate and compare their performances. The lack of sound experimental evaluation makes it difficult to assess the state of the art, particularly those aspects of a problem still requiring improvement. The essential elements of framework for comparison of algorithms are problem definition, objective performance measures, and large sets of images with ground truth.

In this paper we evaluate and compare eight shading correction methods. For evaluation three sets of simulated and two sets of real images were used. A RCS method to be effective should correct the shading when present, but should not corrupt the shading-free images. The performance of RSC algorithms was quantitatively measured by the change of the coefficient of intensity variations in different object classes. All images used in this paper are available via: *http://biprog.fe.uni-lj.si /shading/images*

2. Methods

In this section we formulate the problem of shading correction and provide an overview over the retrospective shading correction methods.

2.1. Problem formulation

The formation of an image $N(x,y)$ is an interaction between objects in real space, illumination, the optical system, and the sensor. In transmission microscopy, the interaction between an object and illumination may be described by the absorption model:

$$N(x,y) = I(x,y) \cdot e^{-l(x,y)\cdot D(x,y)} \tag{1}$$

while in reflectance microscopy, the interaction is described by the reflectance model:

$$N(x,y) = I(x,y)R(x,y) \tag{2}$$

$I(x,y)$ represents the illumination, $D(x,y)$ is the object thickness, and $l(x,y)$ and $R(x,y)$ are the imaged absorption and reflectance, respectively, of an object.

If $I(x,y)$ and $D(x,y)$ do not depend on (x,y), i.e., $I(x,y)=I$ and $D(x,y)=D$, a shading-free image $U(x,y)$ is acquired:

$N(x,y)=U(x,y)$. Otherwise, the relation between an intensity inhomogeneous acquired image $N(x,y)$ and its corresponding shading-free image $U(x,y)$ may be well described by the following linear model:

$$N(x,y) = U(x,y)S_M(x,y) + S_A(x,y) \quad (3)$$

where $S_M(x,y)$ and $S_A(x,y)$ are the multiplicative and the additive shading components, respectively [2]. These two components also encounter the shading caused by the optical system and the sensor. Shading correction is concerned with deriving the shading-free image $U(x,y)$ from the acquired image $N(x,y)$. If the shading components $S_M(x,y)$ and $S_A(x,y)$ are known, shading correction may be achieved by inverting the linear model (Eq. 3):

$$U(x,y) = \frac{N(x,y) - S_A(x,y)}{S_M(x,y)} \quad (4)$$

The shading correction problem is often oversimplified by assuming that only one of the shading components, either $S_M(x,y)$ or $S_A(x,y)$, is involved in the corruption of the image $U(x,y)$. In such a case, shading correction is performed either as:

$$U(x,y) = N(x,y) - S_A(x,y) + C \quad (5)$$

or as:

$$U(x,y) = \frac{N(x,y)}{S_M(x,y)} C \quad (6)$$

where C is the normalisation constant needed to restore the desired grey level range. If shading is object-independent, $S_M(x,y)$ or/and $S_A(x,y)$ may be obtained by the acquisition of one or two additional calibration images (e.g. by recording an empty or defocused microscopical field and by taking an image with the shutter closed) [8]. However, object-dependent shading requires a retrospective correction, i.e., the shading components $S_A(x,y)$ or/and $S_M(x,y)$ must be derived from the acquired image $N(x,y)$.

2.2. Retrospective shading correction techniques

2.2.1. Linear filtering. Linear filtering [1,2] assumes that only the additive component $S_A(x,y)$ is present in the image $N(x,y)$ and that it can be determined by low-pass filtering (LPF) of the acquired image:

$$S_A(x,y) = LPF\{N(x,y)\} \quad (7)$$

Shading correction is then performed by using Eq. 5.

2.2.2. Homomorphic filtering. This technique [2,4] involves low-pass filtering of the logarithm of the acquired image and thus derives solely the multiplicative shading component $S_M(x,y)$:

$$S_M(x,y) = \exp\{LPF\{\log\{N(x,y)\}\}\} \quad (8)$$

Eq. 6 is then used to correct the image $N(x,y)$.

A key to the efficient correction by both methods is in the selection of an appropriate low-pass filter by which the spectra of shading and shading-free data are to be separated.

2.2.3. Morphological filtering. The assumption behind morphological filtering is that objects of interest are limited in size and smaller than the scale of background variations, and that the background is everywhere either darker or lighter than the objects [2]. If this assumption holds, greyscale morphology operators [5] may be used to filter out the objects and thus obtain an estimation of the background. This may represent either $S_A(x,y)$ or $S_M(x,y)$ and Eq. 5 or 6, respectively, is used for correction. The size of the structuring element should be slightly larger than the size of the objects that are to be filtered out.

2.2.4. Fitting a shading model. By selecting a number of points in the background or in an object class, a list of intensity values and locations can be acquired. The intensity variation over the image background or object class may be obtained by least-squares fitting of a function $F(x,y)$ to the intensity values at the pre-selected points. Most often the function $F(x,y)$ is a second order polynomial [1,3]:

$$F(x,y) = a_0 + a_1x + a_2y + a_3x^2 + a_4y^2 + a_5xy \quad (9)$$

The function $F(x,y)$ may either represent $S_A(x,y)$ or $S_M(x,y)$ and Eq. 5 or 6, respectively, is then used for shading correction. Alternatively, two parametric functions can be used. For example, the function $F_D(x,y)$ may be fitted to intensity values at points belonging to a dark object class, while $F_B(x,y)$ is fitted to intensity values of a bright object class. In this case, both shading components may be derived:

$$S_M(x,y) = \frac{F_B(x,y) - F_D(x,y)}{\overline{F_B} - \overline{F_D}} \quad (10)$$

$$S_A(x,y) = F_D(x,y) - \overline{F_D} S_M(x,y) \quad (11)$$

where $\overline{F}$ denotes the mean value of the function $F(x,y)$ in the image domain.

A crucial step in this approach is the selection of the representative points [1]. Manual selection of points, which is subjective and time-consuming, calls for an automatic approach. A straightforward way in this direction is to subdivide the image into a grid of smaller rectangles. In each rectangle a point is then selected, which has the *mean*, *median*, *minimum*, or *maximum* grey value. In the same way two points may be selected in each rectangle, for example, the *minimum* and *maximum*, and used for fitting two functions. The robustness of fitting may be improved by detecting and removing the points that show significant inconsistency with respect to the fitting function.

2.2.5. Entropy minimisation. In the method recently proposed by Likar and Pernuš [3], it is assumed that shading (Eq. 3) increases the level of uncertainty in the image, which is quantitatively expressed by entropy. Shading correction, which is a search for the optimal corrected image $U_o(x,y)$, is performed by modelling the shading components $S_M(x,y)$ and $S_A(x,y)$ by the second order polynomials and varying their parameters until the entropy H of the image $U(x,y)$ (Eq. 4) reaches a minimum:

$$U_o(x,y) = \arg\min_{U(x,y)} \{H(U(x,y))\} \quad (12)$$

3. Experiments and results

In this section we first describe the procedure for computer generation of artificial images and outline the acquisition set-ups for capturing real microscopical images. Next, we specify the implementation details of the shading correction methods and show their performances on artificial and real microscopical images.

3.1. Artificial images

Three sets of twenty differently structured artificial images were generated. The images in all three sets were 400x400 pixels, 8 bit. Those from the first set contained small (mean area = 100 pixels) dark and bright objects over a uniform background, the images from the second set contained dark and bright medium-sized (mean area = 2000 pixels) objects separated by thin brighter segments, while the images in the third set contained larger (mean area = 20000 pixels) objects belonging to four different classes. To each object class a different amount of noise was added with standard deviations ranging from 5 to 10 grey levels.

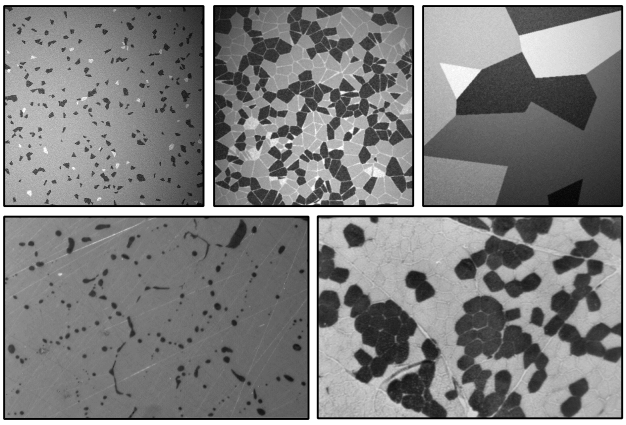

Figure 1. Top row: The examples of shaded artificial images from the set of small (left), medium (middle), and large (right) sized objects. Bottom row: The examples of real microscopical images of AgSe alloy (left) and muscle fibers (right).

To simulate the effect of shading, the absorption model of image formation (Eq. 1), which is more complex than the reflectance model, was implemented and applied to each of the shading-free image. The illumination $I(x,y)$ was modelled by a smooth cosine function:

$$I(x,y) = \cos\left(w\sqrt{(x-x_o)^2 + e^2(y-y_o)^2}\right) \quad (13)$$

while the thickness $D(x,y)$ was modelled by a second order polynomial. The parameters of the polynomial and w, e, x_0, and y_0 were selected randomly for each image. In this way, three sets of shading-free and corresponding shaded copies were obtained. Typical examples of shaded artificial images from each set are illustrated in Figure 1.

3.2. Real images

Two sets of twenty microscopical images were used. The first set contained images of silver and selenium alloys (AgSe) acquired by the reflectance technique, while the second set contained muscle fibre images obtained by the transmission technique (Figure 1).

The first set (AgSe alloys) was obtained by an Olympus BX-40 microscope, Sonny SSC-M370 CCD camera, and a Matrox Meteor frame grabber (680x512 pixels, 8bit). The second set (muscle fibres) was acquired 7 years ago by an Opton photomicroscope, while the photographs were captured recently by a Sony XC-77CE CCD video camera, equipped with Ultrak CCTV lens 25mm-1.4f, and digitised by a Matrox Meteor frame grabber (760x512 pixels, 8 bit). A typical image of each set is illustrated in Figure 1.

3.3. Implementation details

We implemented eight methods for retrospective shading correction, i.e., linear filtering (LF), homomorphic filtering (HF), morphological filtering with additive correction (MFA), morphological filtering with multiplicative correction (MFM), fitting a second order polynomial and additive correction (FA), fitting a second order polynomial and multiplicative correction (FM), fitting two second order polynomials and applying both additive and multiplicative correction (FB), and the entropy minimisation method (EMI).

In the LF and HF method the filtering was performed in the frequency domain by the convolution with a Gaussian-shaped filter with standard deviation s.

In the MF method the combination of *opening* and *closing* operation was used for the first set of artificial images and for the AgSe images, while only *closing* was implemented for the second set of artificial images and for the muscle fibre images. The structuring element in *opening* and *closing* was a square of size L_O and L_C, respectively. Prior to shading correction, the outcome of morphological filtering was convolved with a uniform-squared mask of size L_C.

In the FA, FM, and FB method, the images were subdivided into a gird sub-images, each *GxG* pixels large. In the FA and FM method, local *medians* were used as the representative points in the first set of artificial images and in the AgSe images, while local *maxima* were used for the same task in the second set of artificial images and for the muscle fibre images. In the FB method local *minima* and local *medians* were used as representative points for fitting the two models in the images of the first set of artificial images and AgSe images, while local *maxima* were used instead of local *medians* for the same purpose in the second set of artificial images and in the set of muscle fibre images. When the FA, FM, and FB methods were applied to real microscopical images, the following two-step procedure for removing the inconsistent points was used:

1. Fit the function $F(x,y)$ to the set S of selected points, determine the differences d_i between the derived

model and each selected point, and compute the corresponding standard deviation s_d.

2. If s_d is larger then a pre-selected s_v: Remove the point with the largest distance d_i from the set S and go to the first step; else: Stop.

The EMI method was implemented as described in [3] with no modifications.

All methods except EMI require a selection of a certain number of parameters on which their performances depend. The optimal parameters were found after substantial experimentation so that all algorithms were treated equally. The implementation parameters that yielded the best performances of each method are summarised in Table 1. Because none of the methods, except the EMI, could correct the shading present in the third set of artificial images, no parameters are given for this set. The same holds for the LF and HF methods when applied to muscle fibre images.

Table 1. Implementation parameters

		Artificial images			Real images	
Method	**Parameters**	**Set 1**	**Set 2**	**Set 3**	**AgSe**	**Muscle**
LF	s	30	80	NAP	50	NAP
HF	s	40	80	NAP	50	NAP
MFA	L_O, L_C	13, 27	-, 50	NAP	10, 20	-, 120
MFM	L_O, L_C	13, 27	-, 50	NAP	10, 20	-, 120
FA	G , s_v	50, -	50, -	NAP	50, 5	80, 5
FM	G, s_v	50, -	50, -	NAP	50, 5	80, 5
FB	G, s_v	50, -	50, -	NAP	50, 5	80, 5
EMI	-	-	-	-	-	-

NAP - No Appropriate Parameters

3.4. Performance evaluation

Each method was tested on shading-free and shaded artificial images and on real images. The performances of shading correction methods were evaluated both qualitatively and quantitatively. Qualitatively, the performance was determined by visually evaluating the results of shading correction. The methods, which yielded completely useless results on a particular set of images, regardless of the parameters used, were not quantitatively evaluated.

Quantitatively the performance of each method was expressed by the reduction/increase of intensity variations within the objects of the same class after shading correction. For this purpose the coefficient of variations, defined as the standard deviation divided by the mean grey value, was calculated before and after correction for two different object classes, both in the sets of shading-free and shaded images. Such a test requires a shading-tolerant segmentation of object classes, which was trivial in the case of artificial images. For the real microscopical images a coarse segmentation was conducted by manually pinpointing the centres of the individual objects, i.e. dark spots (selenium), background regions (silver), dark fibres and bright fibres. The radii of circular regions were visually established so that they were completely inside the objects that they represented.

The results of shading correction methods, applied to the first two sets of artificial shaded and shading-free images, and the two sets of real microscopical images, were expressed by the percentage of reduction of the coefficient of variations and illustrated by box-whiskers diagrams, showing the minimum, maximum, median, and 1st and 3rd quartile of the distribution of twenty samples.

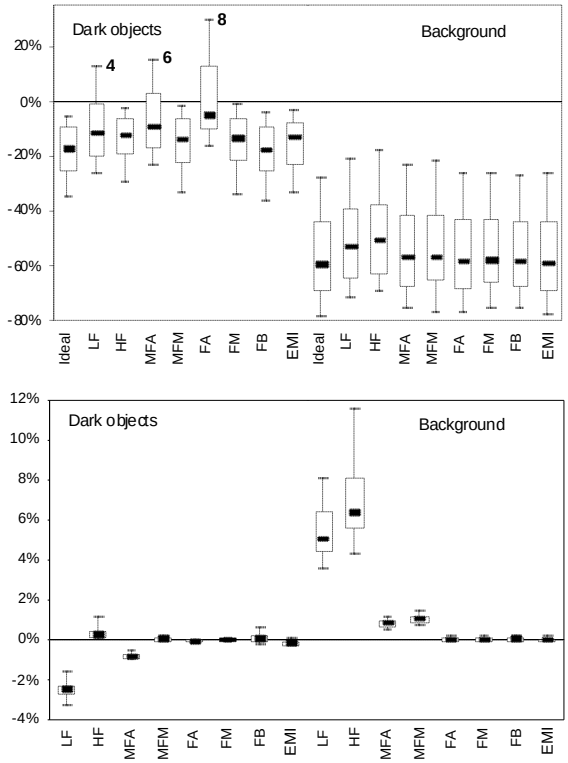

Figure 2. The change of the coefficient of variations after shading correction of shaded (top) and shading free (bottom) artificial images from the first set.

3.5. Results

The top diagram in the Figure 2 shows the changes of the coefficients of variations of the dark objects and background in the shaded artificial images of the first set, while the corresponding changes in the shading free artificial images are presented in the bottom diagram. Similarly, Figure 3 shows the changes of coefficient of variations in the shaded and shading-free artificial images from the second set. In Figures 2 and 3 the distributions of changes of the coefficients of variations, which would be obtained by an ideal method, are given. These changes were computed from the shaded and corresponding shading-free images.

In Figure 2, it can be observed that nearly all methods reduce the intensity variations within dark objects and background. No significant distinction between the eight methods was found, although the LF, MFA and FA methods yielded an increase of dark objects intensity variations in 4, 6, and 8 images, respectively. The FB and

EMI methods yielded the distributions of changes of coefficient of variations that were the most similar to the ideal distribution. In the bottom diagram (Figure 2), one can see that only the FA, FM, FB, and EMI methods do not change the intensity variations of the shading-free images.

Figure 3 shows that on medium-sized objects the FB and EMI methods performed the best, i.e., yielded the highest reduction of the intensity variations of the dark and bright objects. The MFA and FA methods significantly increased the intensity variations of dark objects in the shaded images. For the EMI method the distributions of changes of coefficient of variations is the most similar to the ideal distribution. All methods, except EMI, when applied to the shading-free images, increased the intensity variations.

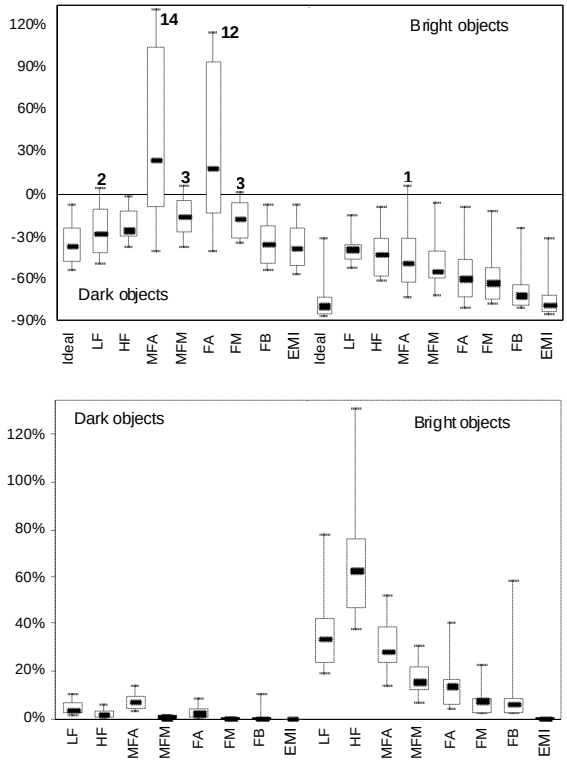

Figure 3. The change of the coefficient of variations after shading correction of shaded (top) and shading free (bottom) artificial images from the second set.

The EMI method was the only one that yielded good corrections of the large-structure images from the third set, although it failed in four out of twenty shaded images, most likely because of finding a local instead of the global entropy minimum. The median change of variations achieved was -54.8% and -31.1% for dark and bright objects, respectively. The EMI method, applied to the large-structured shading-free images, did not induce additional intensity variations.

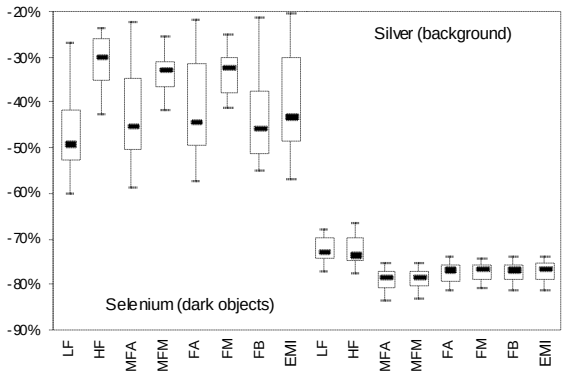

Figure 4. The change of the coefficient of variations after shading correction of AgSe alloys images.

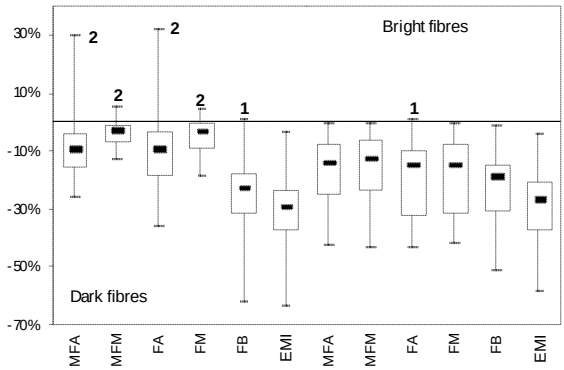

Figure 5. The change of the coefficient of variations after shading correction of muscle fibres images.

The results of shading correction methods, applied to AgSe alloy images (Figure 4), show that each of the eight methods significantly reduce intensity variations within both selenium (dark objects) and silver (background), and that non of the method significantly outperforms the others.

Figure 5 illustrates the results of six correction methods that yielded meaningful results on muscle fibre images. It can be seen that the FB and EMI methods outperformed the others. This is due to the presence of both the additive and multiplicative shading components in this set of images. The EMI method slightly outperformed the FB method.

Table 2. Performance (+ good, o average, - poor) of correction methods for different image sets.

	Methods							
Image set	**LF**	**HF**	**MFA**	**MFM**	**FA**	**FM**	**FB**	**EMI**
Set 1	o	+	o	+	o	+	+	+
Set 2	+	+	o	+	o	+	+	+
Set 3	-	-	-	-	-	-	-	+
AgSe	+	+	+	+	+	+	+	+
Muscle	-	-	o	+	o	+	+	+

With regard to their performance, we have classified the methods into those whose performance was poor (-), average (o) or good (+) (Table 2). As such, Table 2 may assist the operators, facing the shading correction problem, in choosing the appropriate method for a given task.

4. Discussion

Shading correction tries to recover the shading-free images from the intensity inhomogeneous ones. In this paper we implemented eight retrospective shading correction algorithms in order to compare their performance in terms of reduction of intensity variations. The algorithms come from four groups; the grouping is based on conceptual differences among the algorithms. The comparison was carried out on three sets of synthetic shading-free and corresponding shaded images and on two sets of real microscopical images. The results show that none of the algorithms, except the algorithm based on entropy minimisation, performs consistently for all image sets. They work well for certain images, but performed poorly for others.

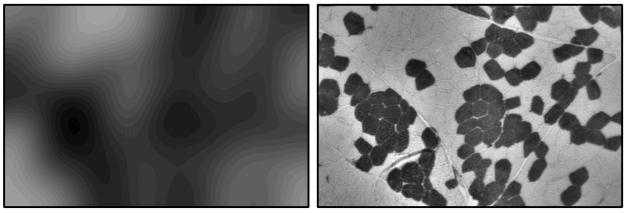

Figure 6. $S_M(x,y)$ component (left) extracted with Gaussian filter ($s=100$) from muscle fibre image from Figure 1, and the corresponding corrected image (right).

The filtering methods (LF, HF, MFA, and MFM) are most suitable for correcting images of small objects. In other words, the spectra of the true image data and shading should not overlap and can thus be separated by simple filtering (LF and HF), or alternatively, the objects should be small enough so that they can be removed by morphological filtering (MFA and MFM). Even if the above requirements are met, the operator must select a number of parameters, such as width, size, and/or shape of the filter or structuring element. This is not always a straightforward task but usually requires substantial manual tuning. Still, the filtering approach may not always yield meaningful results, as shown Figure 6, where the overlapping spectra of shading and true data can not be efficiently separated. Alternatively, the morphological filtering approach may in some cases efficiently remove the objects from the background, even if the spectra are overlapping. Unfortunately, this approach generally fails on images containing large objects. An example of morphological filtering artefacts is illustrated in Figure 7.

Fitting methods (FA, FM, and FB) performed well on images containing small and medium sized objects. The methods applied to artificial images required no robust fitting, because local intensity distributions, from which the control points were derived, were affected solely by the simulated shading. In real microscopical images, other anomalies are generally present and affect local intensity distributions and automatic control point selection. Consequently, robust fitting is strongly recommended in real images. The proposed robust fitting of two parametric functions (FB method) outperformed its two counterparts that fit a single component, confirming the presence of the two shading components in the real microscopical images and the need of their retrospective correction.

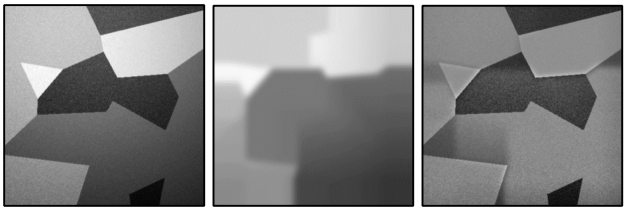

Figure 7. Original artificial image (left), $S_M(x,y)$ component (middle) extracted by morphological filtering ($L_O=100$), and the corresponding corrected image (right).

The method based on entropy minimisation (EMI) also addresses both shading components and seems to be the most general, as illustrated by the results of its application to a variety of differently structured artificial and real microscopical images. Besides, the EMI method requires no operator-specific tuning and does not induce spurious intensity variations to the shading free images.

In conclusion, let us cite Jain and Binford [6]: "The importance of theory cannot be overemphasized. But at the same time, a discipline without experiment is not scientific. Without adequate experimental methods, there is no way to rigorously substantiate new ideas and to evaluate different approaches." This paper is a contribution in this direction.

5. References

[1] J.C. Russ. *The image processing handbook*. Second Edition, IEEE Press, Boca Raton, 1995.

[2] V.K. Madisetti and D.B. Williams. *The digital signal processing handbook*. CRC Press, Boca Raton, pp. 51-62 – 51-66,1998.

[3] B. Likar and F. Pernuš. *Retrospective shading correction of microscopical images.* Czech Pattern Recognition Workshop 2000.

[4] S.E. Umbaugh. *Computer vision and image processing*. Prentice-Hall, New York, 1998.

[5] R.M. Haralick, S.R. Sternberg and X. Zhuang. Image Analysis Using Mathematical Morphology. *IEEE Trans. Pattern Anal. Machine Intell.* 9: 532-550, 1987

[6] R.C. Jain and T.O. Binford. Ignorance, Myopia, and Naivete in Computer Vision Systems, *CVGIP*, vol. 53-1, pp. 112-117, 1991.

[7] S. Inoué. *Video microscopy*. Plenum Press, New York, 1986.

[8] D.E. Wolf. Quantitative video microscopy. *Method. Cell. Biol*. 56:117-134, 1998.